Research Article

Esteban Broitman, Dumitru Nedelcu*, and Simona-Nicoleta Mazurchevici

Tribological and nanomechanical properties of a lignin-based biopolymer

https://doi.org/10.1515/epoly-2020-0055
received August 16, 2020; accepted August 27, 2020

Abstract: A research is reported on the nanomechanics and tribology of the Arboblend V2 Nature biopolymer (a 100% bio-based material, biodegradable, or resistant depending of application), being a mixture of different biopolymers such as lignin, polylactic acid, cellulose, biopolyamides, and other natural additives. The specimens were made by an industrial-scale injection molding machine. The nanoindentation characterization have unveiled that an increase in processing temperature from 160°C to 170°C produces a rise in hardness and elastic modulus of ~20%. Tribological characterization against a bearing-steel counterface has shown that for both processing temperatures, the increase of the applied load or the increase of sliding speed will produce an increase of the friction coefficient (μ) and wear. At an applied load of 1 N (contact pressure of 104 MPa) and tracks in a direction perpendicular to the surface textured lines, the lowest $\mu \sim 0.148$ are for samples made $T = 170$°C, while for tracks parallel to the textured lines, the lowest $\mu \sim 0.059$ is obtained for samples made at $T = 160$°C. Experiments made at different ambient humidity have established that friction coefficient is higher at 0% RH or at 75% RH than at 33% RH. Our results show that the biopolymers Arboblend V2 Nature is a candidate to substitute some popular fossil-based thermoplastics in numerous tribological industrial applications.

Keywords: biopolymers, lignin, Arboblend V2 Nature, nanoindentation, wear, friction

*** Corresponding author: Dumitru Nedelcu,** Department of Machine Manufacturing Technologies, "Gheorghe Asachi" Technical University of Iasi, 700050, Iasi, Romania,
e-mail: nedelcu1967@yahoo.com
Esteban Broitman: SKF – Research & Technology Development Center, 3992 AE Houten, The Netherlands,
e-mail: esteban.daniel.broitman@skf.com
Simona-Nicoleta Mazurchevici: Department of Machine Manufacturing Technologies, "Gheorghe Asachi" Technical University of Iasi, 700050, Iasi, Romania,
e-mail: simona0nikoleta@yahoo.com

1 Introduction

Developing and production of bio-based polymeric materials has increased during the last two decades, due to the recommendations about using green materials to substitute fossil-based materials (1). Thermoplastics with competitive tensile properties made with lignin, a natural biopolymer found in vegetal fibers, were first reported by the University of Minnesota in 1995 (2) and is nowadays used mixed with synthetic polymers to produce copolymers, composites, and other kinds of blends (3). Lignin is also used to functionalize polymers in many fields like foams, adhesives, and coatings (4).

Arboblend V2 Nature is the trade name of a mixture of lignin (>90%), plus other organic additives like starch, waxes, natural resins, and strengthening natural fibers (1). This biopolymer belongs to a group of polymers technically known as "liquid wood," which were developed by researchers of Fraunhofer-Institute for Chemical Technology (ICT) in Pfinztal (Germany) and later started to be commercialized by Tecnaro GmbH (5). Many methods can be used to produce Arboblend V2 Nature polymers like film, sheet, profile extrusion, blow molding, thermoforming, and 3D-printing. The mentioned diversity of methods has given place to the manufacture of precision parts (6), stacking aids for the transport of solar cells (7), building structures (8), forest plates (7), different kind of toys (9,10), furniture and decorative items (11), watch cases (12), and musical instruments and loudspeakers (13). Arboblend V2 Nature has an amorphous structure and can be considered a thermoplastic with a melting temperature starting at $T = 104$°C, while at $T = 142$°C the entire mass of material is almost melted, and around 460°C, the whole material vaporizes (14).

Despite the high interest in the use of biopolymers, there is still a small amount of scientific investigations reporting mechanical properties (hardness and elastic modulus) and tribological properties (friction and wear) of Arboblend V2 Nature material. The publications by Fraunhofer ICT were the first to report their mechanical

properties: yield stress of 49.5 N/mm^2 and yield strain of 2.33%; elastic modulus (tensile) of 2.74 GPa (1). Researchers at "Gheorghe Asachi" Technical University of Iasi (Romania) has a tradition investigating biopolymers. Nedelcu et al. reported the tensile strength of Arboblend V2 Nature specimen as 44 MPa and tensile strain at fracture of 4.9% (15), modulus of elasticity (in flexion) of 1.7 ± 0.2 GPa (16), microhardness in the range 110–140 MPa (17), and reduced elastic modulus of 1.42–2.62 GPa (17). Furthermore, a dry friction coefficient in the range 0.14–0.16 has been reported for an Arboblend V2 Nature pin against AISI 572 Gr 65 (OL60) steel disk (15).

In a previous publication, we have compared the nanomechanical and tribological properties of another "liquid–wood" polymer named Arboform, and reinforced with aromatic polyamide (Aramid) fibers (18), which have a nonrenewable fossil origin. Arboform has only 30% of lignin, being the rest comprised of wood pulp fibers and other natural additives. Although it is not a real 100% biopolymer because of the Aramid reinforcement fibers, and despite of a relatively high friction coefficient of $\mu \sim 0.4$ in most of the cases, the material demonstrated to have the potential to replace fossil-based polymers in many applications.

In this paper, we study the nanomechanical and tribological properties of the natural biopolymer Arboblend V2 Nature that contains more than 90% lignin. The specimens were produced in an industrial-scale commercial injection molding machine. Hardness and elastic modulus were determined by the nanoindentation technique. Friction characteristics against a bearing steel ball were measured by a reciprocating test at loads between 1 and 10 N, speeds in the range 2.5–50 mm/s, and relative humidity (RH) environments from 0 to 75% RH.

2 Materials and methods

Samples were prepared using a SZ-600H industrial-scale injection molding machine. Arboblend V2 Nature specimens were produced by using pellets Arboblend V2 Nature manufactured by Tecnaro in Germany. The pellets were placed in a chamber under hot air drying for 4 h. Afterward they were introduced in a bunker at the equipment waiting to enter into the injection cylinder, heated electrically in the range 160–170°C following a prerecorded process, and then injected into a specially designed mold that was being water cooled at a temperature of 23°C. In a previous study (15), the process key parameters, such as injection time (11 s) and injection pressure (100 MPa), were studied and optimized. Two series of specimens were prepared, injected at two different melting temperatures (160°C and 170°C), and injection angle of 0° by using the injection mold shown in Figure 1.

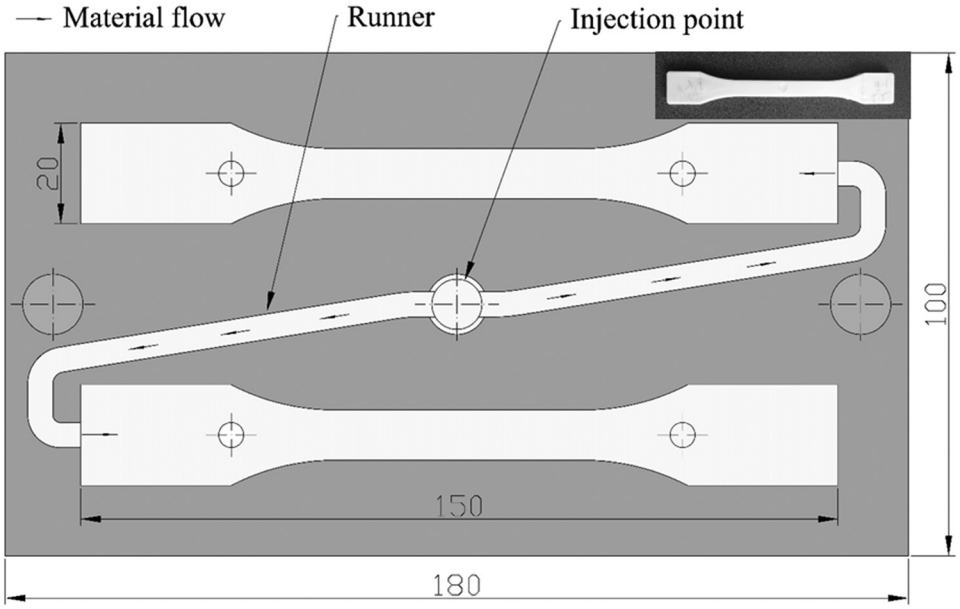

Figure 1: Top view schematic of the injection mold, with an injection angle of 0°. The arrows show the melted material flow; indicated sizes are in mm (adapted from (18)).

The nanoindentation hardness (H_{IT}) and reduced Young's modulus (E_r) were studied by using a Triboindenter TI950 (Hysitron Inc, nowadays Bruker, USA). The nanoindentations were done with a Berkovich diamond indenter at loads applied in the range 2–8 mN. The nanoindentation experiments were conducted under a penetration-controlled feedback, being the indenter maximum penetration depth held at 1,000 nm for all samples. Using the unloading elastic portion of the load–displacement curve, H_{IT} and E_r were determined using the Oliver and Pharr's method (19). Twelve indentations were made per sample to determine a mean value and its error. In order to avoid the presence of creep originated from the polymer viscoelasticity, we used fast load/unload rates in the range of 0.4–1.6 mN/s (20).

The elastic modulus of the polymer, E, was calculated from the reduced elastic modulus E_r by using the relation:

$$\frac{1}{E_r} = \frac{1-\nu_i^2}{E_i} + \frac{1-\nu_p^2}{E} \quad (1)$$

where E_i = 1,140 GPa is the Young's modulus and ν_i = 0.07 is the Poisson's ratio of the diamond indenter. The Poisson's ratio ν_p for the Arboblend V2 Nature materials is assumed to be 0.38, as recommended by Constantin et al. (21).

The tribological characterization was done by utilizing a tribometer (Tribotechnic, France). In our experiment, we designed a reciprocating tribotest consisting of a "ball against a flat sample" configuration. A 6.35 mm diameter AISI 52100 (SKF) bearing steel ball was selected as a representative counterpart for the experiments because it is assumed that polymeric components are usually in contact against steel materials in many technological applications. The ball performed a reciprocating movement with a stroke distance of 5 mm, and a total number of 3,000 cycles. The "flat samples" of the tribological pair were our Arboblend V2 parts cut from the specimen shown in Figure 1 in a size of 20 mm × 20 mm. We repeated the tests at least three times for each tribological situation, being the compared friction reported results as the typical for the sample and condition.

Load-dependence tests were done at five different loads (L): 1, 2, 3, 6, and 10 N. Furthermore, experiments at L = 3 N were repeated at five different sliding speeds of 2.5, 5, 10, 20, and 50 mm/s. Friction humidity tests were realized by varying the RH inside the environmental chamber housing the tribometer. RH values of 33% and 75% were achieved by the use of prepared saturated salt solutions of $MgCl_2$ and NaCl, respectively (22). For obtaining the RH = 0%, the chamber was filled up with dry nitrogen at 1 atm. Experiments, done at L = 3 N and repeated three times, were started after the humidity was stable in the chamber for at least 60 min. Temperature and humidity in the tribometer chamber were monitored during all the experiments by using the computerized tribometer sensors (temperature error: ±0.1°C; humidity error: ±0.1% RH).

An optical microscope (400×) was used to inspect the wear tracks, which were further measured at the nanometer scale by a profilometer (DektakXT – Bruker).

3 Results and discussion

3.1 Morphology

Figure 2 displays the photomicrographs of Arboblend V2 Nature samples made at 160°C and 170°C. The specimens exhibit a textured surface consisting of groove-like

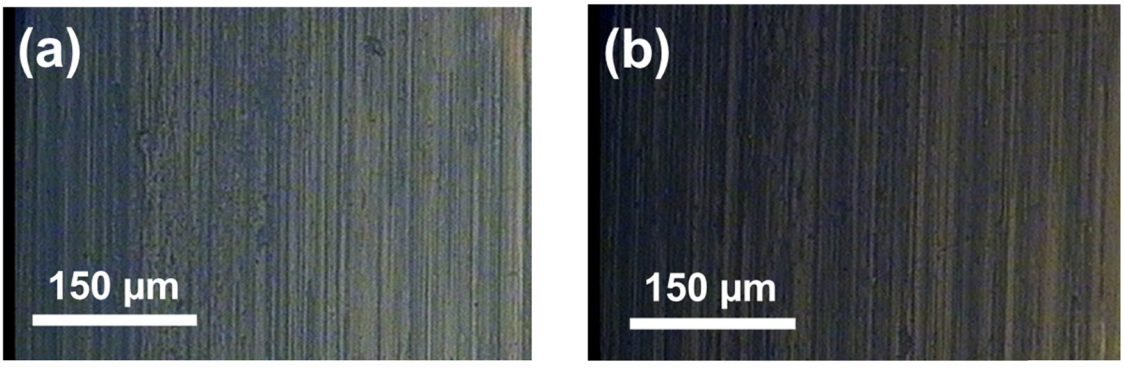

Figure 2: Optical microscopy of Arboblend V2 Nature samples made at (a) 160°C and (b) 170°C.

Table 1: Surface roughness parameters for the samples

Temperature (°C)	Direction	R_a (nm)	W_t (nm)
160	∥	73 ± 3	266 ± 4
160	⊥	78 ± 3	1,023 ± 27
170	∥	90 ± 4	279 ± 4
170	⊥	91 ± 4	1,052 ± 28

equal-spaced lines parallel to the injection direction. Surface roughness measured along a 5 mm length distance in parallel and perpendicular directions to the texture lines can be used to compare the samples made at both temperatures.

The observed feature in Figure 2 is not a replication of the metal mold surface into the plastic specimens (23), but it is probably due to the injection molding design, as indicated in Figure 1. It is well known that the morphology of the polymers in the moldings is influenced by the process variables like mold and melting temperature, shear forces, applied pressure, and elongational flow (24). We have recently studied the morphological properties of Arboform biopolymers that were made with the same molds of Figure 1 and no textured lines were observed or high waviness W_t values were measured (18). The skin texture in our Arboblend V2 Nature samples is probably due to temperature differences between the bulk and the surface, and the flow field in the molding process. Sawyer has recently demonstrated that, in the skin of many polymers, the lines are the visible part of lamellae orientated parallel to the direction of injection and perpendicular to the mold surface (25).

Table 1 lists two surface roughness parameters: arithmetic average roughness (R_a), and the sum of the maximum valley and maximum peak of waviness profile (W_t) (26). Table 1 reveals that the Ra roughness is influenced by the temperature processing but the waviness W_t seems to have similar values for each direction and sample.

3.2 Nanoscale mechanical indentation

Figure 3 compares the nanoindentation load–displacement curves for Arboblend V2 Nature samples done at 160°C and 170°C, and Table 2 displays their measured hardness and elastic modulus. We never observed a displacement upon load release in the form of a "nose." The existence of such a feature would mean that there is a creep phenomenon during the measurement and invalidate our H and E_r calculations (20,27).

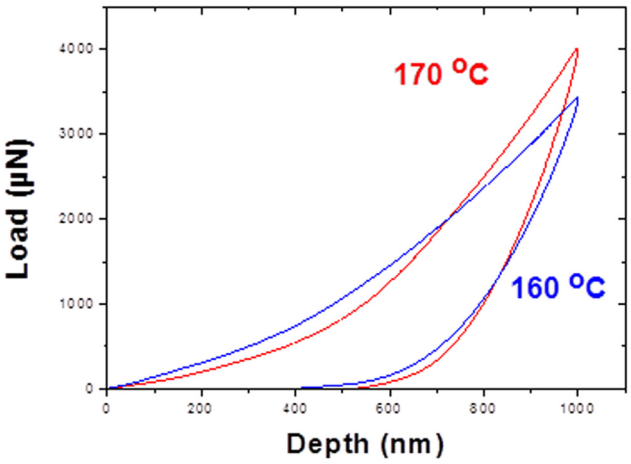

Figure 3: Nanoindentation load–displacement curves for Arboblend V2 Nature samples made at 160 and 170°C.

Table 2: Nanoindentation hardness (H_{IT}) and Young's modulus (E_{IT}) for Arboblend V2 Nature samples made at two temperatures

Temperature (°C)	H_{IT} (MPa)	E_{IT} (GPa)
160	195 ± 18	2.97 ± 0.23
170	230 ± 15	3.60 ± 0.30

Our results unveil that a temperature increase produces an increase in both H and E. The dependence of the mechanical properties with temperature can be correlated with our design of the injection plate (Figure 1). The mechanical properties of the specimen will be driven by the path that the molten biopolymer material gets in, fills up, and cools down inside the cavity. It has been recognized by many researchers that the melt flow grows with temperature rise, resulting in enlarged hardness (28–30). Furthermore, it has also been documented that the elastic properties of the specimens are set by local molecular stretching and by the local structuration attained during the solidification, while the temperature has been reported to have a weak effect (28,31,32).

Only two publications are reporting the hardness of Arboblend V2 Nature material. Manenti measured a macrohardness of 105 N/mm^2 according to ISO 2039 (33), that is determined as the ratio of P_{max} (maximum load) acting on the indenter (steel ball) by the square of impression diameter within 30 s of loading. Nedelcu et al. reported a microindentation hardness of H = 0.11–0.14 GPa (17) by using a load of 10 N and a Rockwell diamond tip of 400 μm diameter. Although our hardness nanoindentation measurements are within alike numeric value ranges, we cannot compare our results with the

values obtained by other authors at macro and microscale. It has been recently discussed that it is very difficult to correlate hardness values measured with different methods and at different scales (27). The comparison of our Arboblend V2 Nature Young's modulus with previously published data using dissimilar characterization methodologies is also not easy. For example, the data measured at the macroscale by flexural tests (E = 1.4–1.9 GPa (16)) cannot be matched up to our nanoindentation tests (Table 1) because during a flexural test the specimen has tensile/compressive deformations within two dimensions, while during nanoindentations we produce compressive deformations in three dimensions (27). Microindentation available Young's modulus data (E = 1.4–2.5 GPa (17)) is also difficult to compare due to different size scale (27). However, we notice that all measurements using various methodologies have values in a similar range.

If we compare the results from Table 2 with our previous results of the pure Arboform polymer (18), with hardness H_{IT} in the range 239–350 MPa and Young's modulus E_{IT} in the range 5.4–5.9 GPa, we conclude that the higher content of lignin in the biopolymer Arboblend V2 Nature (>90%) is probably a slight detrimental factor on its mechanical properties, in comparison to Arboform, which contains only 30% lignin. Interestingly, we will see in the next sections that the biopolymer Arboblend V2 Nature performs tribologically much better than Arboform and the Aramid-reinforced Arboform polymers.

3.3 Tribological characterization

3.3.1 Influence of applied load

Figure 4a and b uncover the friction coefficient μ versus the number of cycles for samples made at 160°C and 170°C, respectively, being the wear track perpendicular to the textured lines of the surface. The specimen displays similar tribological behavior for loads of 1, 3, 6, and 10 N: friction increases with the increased applied load. The friction coefficient for T = 160°C at the start of the experiment is about 0.11, yet within the first 1,500 cycles this value increases rapidly to ~0.2, and afterward μ increases slowly until it reaches a value of approximately 0.21–0.23 at 3,000 cycles. Table 3 shows that the

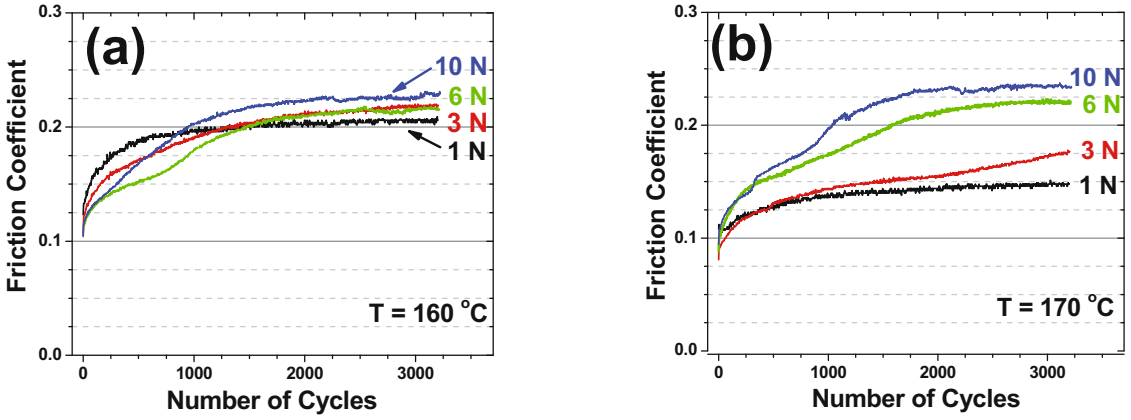

Figure 4: Friction coefficient versus the number of cycles at different loads for samples made at (a) 160°C and (b) 170°C. The wear track is perpendicular to the textured lines of the surface.

Table 3: Final friction coefficients for Arboblend V2 Nature samples measured at different applied loads (L) with the wear track perpendicular (⊥) and parallel (∥) to the surface texture. The mean Hertzian pressure (p_o) is also indicated

Friction direction	T (°C)	L = 1 N p_o = 104 MPa	L = 3 N p_o = 150 MPa	L = 6 N p_o = 189 MPa	L = 10 N p_o = 224 MPa
⊥	160	0.205 ± 0.002	0.216 ± 0.002	0.217 ± 0.002	0.229 ± 0.002
	170	0.148 ± 0.002	0.176 ± 0.002	0.221 ± 0.002	0.235 ± 0.002
∥	160	0.059 ± 0.002	0.119 ± 0.002	0.177 ± 0.002	0.200 ± 0.002
	170	0.109 ± 0.002	0.152 ± 0.002	0.174 ± 0.002	0.210 ± 0.002

final friction coefficient for all loads is within a small spread value. For T = 170°C, the friction values start at about 0.8–0.9, and the running-in also last about 1,500 cycles. However, there is more spread between the friction coefficient at different loads, and the final values range between μ = 0.15 for 1 N and μ = 0.23 for 10 N (Table 2).

We can find only one published research in the scientific literature studying the friction coefficient of an Arboblend V2 Nature pin against AISI 572 Gr 65 (OL60) steel disk, where an average friction coefficient μ = 0.144 was reported (15). Nevertheless, it is impossible to compare this value with the ones obtained in our experiments because that study was done using different measurement techniques (pin-on-disk in rotation mode), pin configuration, counterpart materials, speed, and load. It is well known that a comparison of tribological tests at any scale size should be performed under the same Hertzian contact pressures, speed configurations, and conditions (34).

Wear track observation by optical microscopy (Figure 5) shows that the width of the track width increases, as expected, with the load increase for both sample temperatures. We can also observe the existence of wear debris at the side of the wear tracks, especially at higher loads. Furthermore, visible material damage and few cracks can be visualized at the experiments done at L = 6 N and L = 10 N.

Analysis of the profile tracks (Figure 6) confirms the increase of their width and also the depth with the applied load. Furthermore, the presence of plastic deformation is observed at L = 6 N and L = 10 N. Comparison of the profiles indicates that the sample made at T = 170°C at these higher loads has the highest wear.

Optical microscopy examination of the steel counterpart reveals no obvious wear marks in all tests, or transfer layers, but the presence of certain microparticles on the ball suggests the coexistence of an adhesion mechanism.

It has been recognized that the processes governing polymer friction and wear depends on the applied load ((35) and references therein). At low loads, the elastic surface asperity deformation will control the sliding process with a consequent rise in the friction coefficient with the decreasing of the load (36). At high loads where both plastic deformation at the asperity interactions and thermal softening of the polymer play a role in regulating the real contact area, the friction will increase with the load increase. Therefore, the friction coefficient will go by a minimum value corresponding to the transition from elastic to plastic contact, as described by the theory of Myshkin (36). In our experiments, the observation (Figure 4 and Table 3) that μ increases with the load means that our tribological experiments are done under the plastic contact regime.

It is well known for polymers that the most common wear mechanisms are adhesive and abrasive wear (37). When a steel bearing ball slides against a polymeric material, abrasive wear is produced by the ploughing of the metallic ball asperities onto the polymer surface. Polymer fragments are deposited onto the metal counterpart, which forms a transfer layer. If this transfer layer would remain on the surface, the friction and wear would decrease. Nevertheless, the adhesion of most polymer transfer layers to metal surfaces is known to be very weak and, therefore, the tribological performance of a polymer rubbing against a steel ball will be very poor (37).

Considering the classical Hertz elastic contact problem of a sphere onto an infinite plane (38), it is possible to estimate the overall contact pressure p_0 between the steel ball and the sample as:

$$p_0 = \frac{1}{\pi}\left(\frac{6LE_r^2}{R^2}\right)^{1/3} \quad (2)$$

with the radius for the ball R = 3.15 mm, the reduced elastic modulus E_r calculated from equation (1) with E_s = 213 GPa and ν_s = 0.29 for the AISI 52100 SKF bearing steel ball, and L is the applied load. Average values E_p = 3.3 GPa (from data in Table 2) and Poisson's ratio ν_p = 0.38 (21) were utilized for the specimens. Equation (2) gives contact pressure p_0 values of 104, 150, 189, and 224 MPa for applied loads of 1, 3, 6, and 10 N, respectively, as indicated in Table 3.

It has been confirmed that the contact pressure is responsible for the temperature increase in the tribological contacts of polymers (39). At low p_0, where there is low heating during the tribological test, the polymer wear rate is proportional to the applied contact pressure. However, at a higher p_0 the wear rate suddenly increases, as we observe in Figure 6 for $p_0 \geq$ 189 MPa. Some researchers have speculated that, at high p_0, thermal effects at the contact interface could cause softening or melting at the sliding polymer surface (35).

Figure 7a and b presents the friction coefficient μ versus the number of cycles for samples made at 160°C and 170°C, respectively, being the wear track parallel to the textured lines of the surface. The observed tribological behavior is alike for applied loads of 1, 3, 6, and 10 N: friction increases with the applied load as in the case of perpendicular tracks. However, the samples have

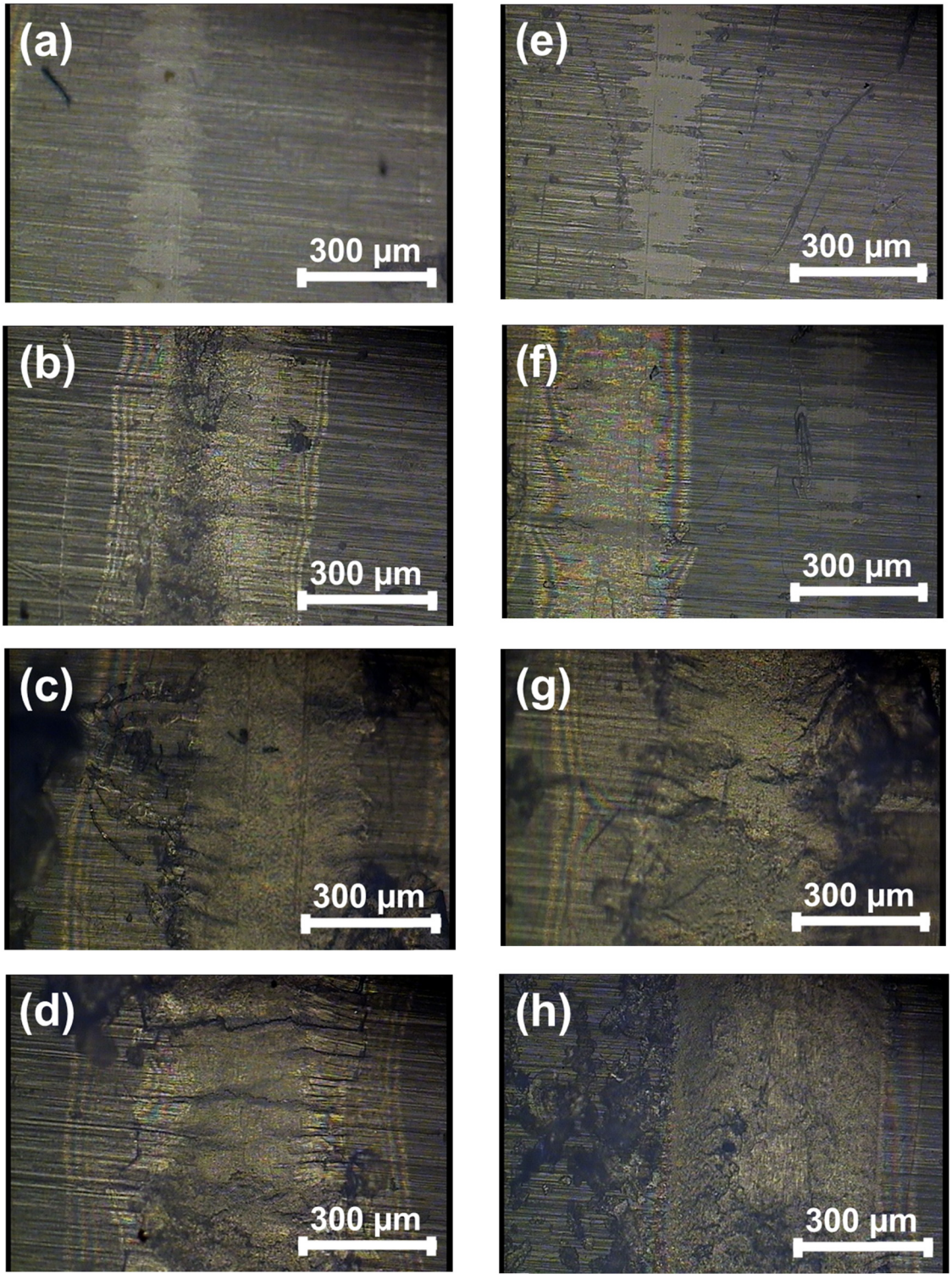

Figure 5: Optical microscopy of wear tracks produced at 1, 3, 6, and 10 N on samples made at $T = 160°C$ (left column: a, b, c, and d) and $T = 170°C$ (right column, e, f, g, and h), respectively. Wear tracks are perpendicular to the textured lines of the surface.

lower values and a marked difference between different loads. Furthermore, the running-in period behavior is very short, 250–500 cycles for lower loads, while samples at higher loads seem that did not arrive to a stable value after 3,000 cycles. Final friction values are also indicated in Table 3.

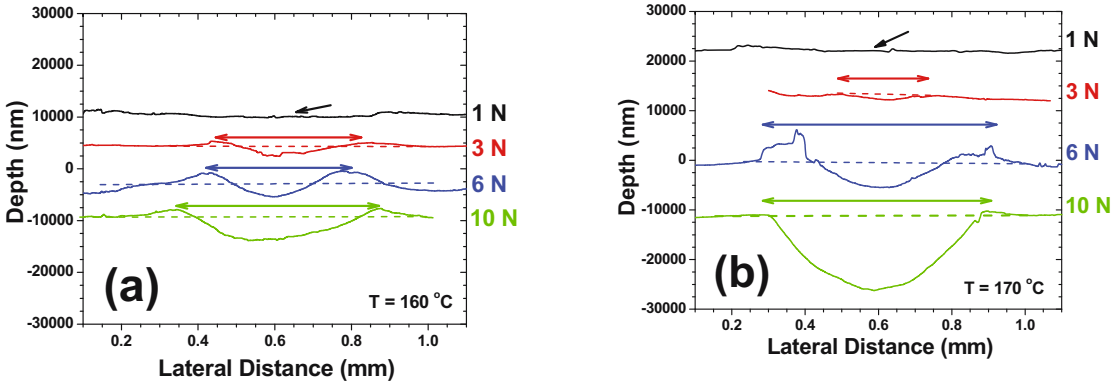

Figure 6: Profile of wear tracks at different loads for (a) sample made at 160°C and (b) 170°C. Wear tracks are perpendicular to the textured lines of the surface.

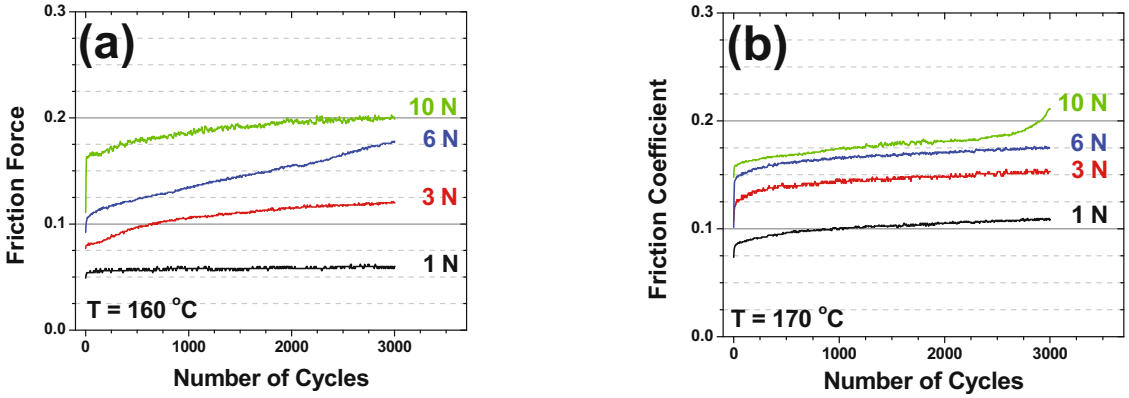

Figure 7: Friction coefficient versus the number of cycles at different loads for samples made at (a) 160°C and (b) 170°C. The wear track is parallel to the textured lines of the surface.

Comparing data in Figures 4 and 5 and Table 3, we conclude that, for tracks in a direction perpendicular to the textured lines, friction is lower for samples made at the higher temperature (T = 170°C) when measured at 1 and 3 N, while is similar for the higher loads. Inversely, for tracks parallel to the textured lines, friction is lower for samples made at the lower temperature (T = 160°C), when measured at 1 and 3 N, and again is about the same for the higher loads. Finally, if we compare all friction results, when we measure at the same conditions, the friction coefficient results always lower for wear tracks parallel to the textured lines.

Wear-track examination by optical microscopy (Figure 8) indicates that tracks parallel to the textured lines have different behavior than samples with a perpendicular track (Figure 5). For both sample temperatures, the track width increases with the applied load. However, we do not observe the presence of wear debris at the side of the wear tracks. Furthermore, visible material damage can be visualized at the experiments done at L = 6 N and L = 10 N only for samples made at T = 160°C.

Friction anisotropy in tribology can involve complicated physical phenomena, but it has been recognized that surface topography plays a crucial role when considering topographical orientation (40). In the case of parallel surface structures (as the ones shown in Figure 2), it has been reported that changes in the sliding direction with respect to the lay of the features have an effect on friction (40,41). For periodical groove-like polymer surfaces consisting of equal lines and spaces, the reports reveal that the friction coefficient in the parallel direction is lower than the friction in the perpendicular one (42,43). The anisotropy is explained not only due to the anisotropic array of the surface structure; the compliance of each surface structure, the material stiffness, and the roughness counterface through a combination interlocking phenomena between

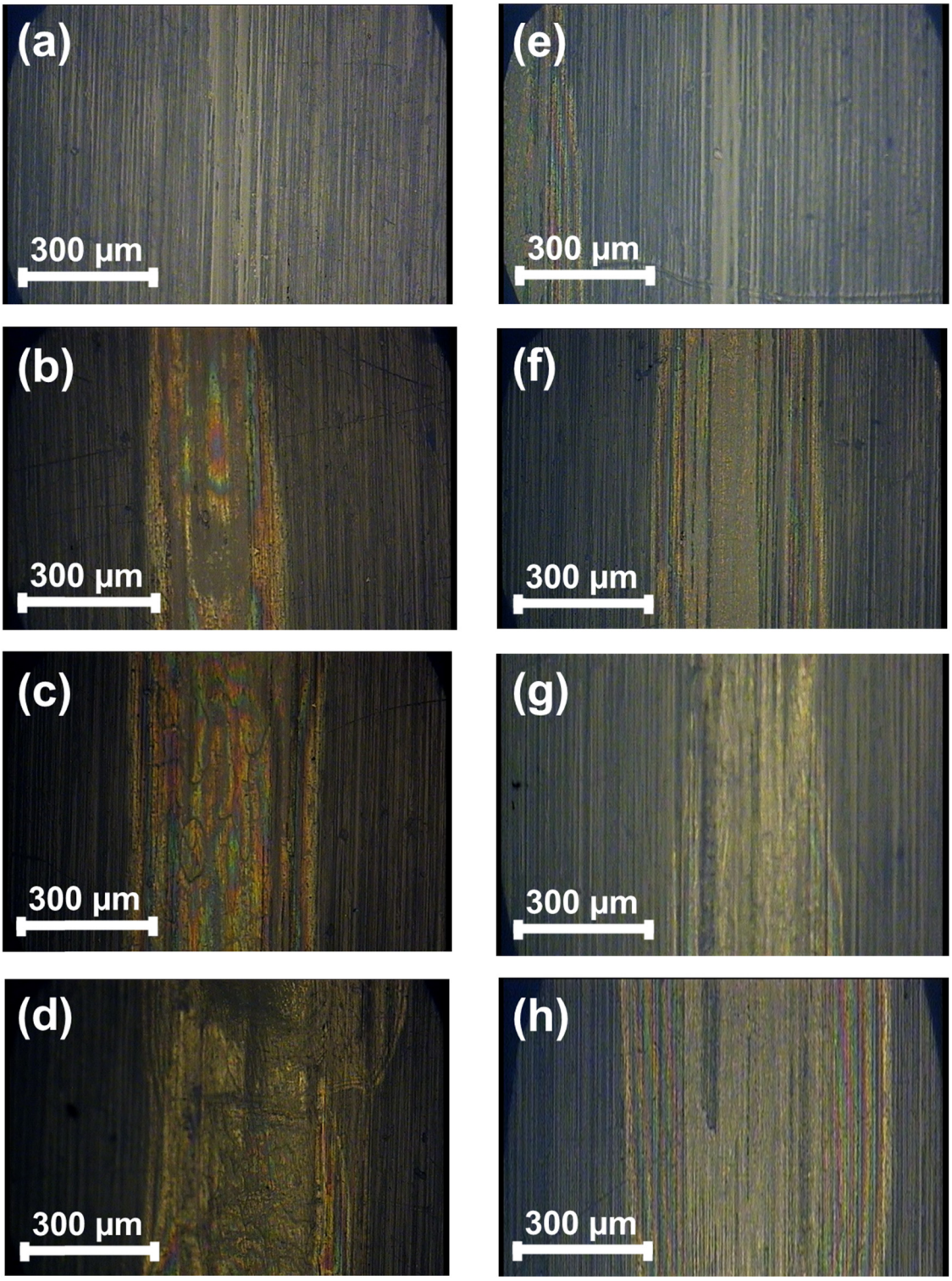

Figure 8: Optical microscopy of wear tracks produced at 1, 3, 6, and 10 N on samples made at $T = 160°C$ (left column: a, b, c, d) and $T = 170°C$ (right column, e, f, g, h), respectively. Wear tracks are parallel to the textured lines of the surface.

the frictional couple and the change of the real contact area also influenced the anisotropy phenomenon ((40–43) and references therein). For both samples in our experiments, the controlling wear mechanism is severe abrasion, resulting in increased ploughing with the load increase (Figure 6). The wear data in that figure

can be used to make a rough estimation of the wear rate k according to Archard's equation (44):

$$k = \frac{h_{wt}}{p_0 S_d} \quad (3)$$

where h_{wt} is the depth of the wear track, p_0 is the Hertzian contact pressure, and S_d is the total slide distance. For the samples done at 160°C, k increases from 0.11×10^{-6} to 0.62×10^{-6} mm^3/Nm when p_0 increases from 104 to 224 MPa, while for the samples done at 170°C, k increases from 0.09×10^{-6} to 2.2×10^{-6} mm^3/Nm. Different publications studying the wear rate of unfilled engineering thermoplastics have shown that at a contact pressure $p_0 \sim 150$ MPa, wear rates values in the range $1–10 \times 10^{-6}$ mm^3/Nm for Polyamide 6, POM, and ultra-high-molecular-weight polyethylene, Poly-methyl-methacrylate (PMMA) ((45–47) and references therein). The lower k values obtained for our biopolymer demonstrate that it could replace fossil-based thermoplastics in many mechanical and tribological applications.

In Section 3.2, we have discussed the possible slightly detrimental influence of the high lignin content on the mechanical properties of the biopolymer. However, if we compare the friction values of Arboblend V2 Nature (with more than 90% lignin) in the range $\mu \sim 0.059–0.239$ with the friction of the polymer Arboform (30% lignin) in the range $\mu \sim 0.456–0.492$ (18), we conclude that the performance of the present high-content lignin biopolymer is greatly superior. In the following sections, we study the behavior of Arboblend V2 Nature at different speeds and different environmental humidity.

3.3.2 Influence of sliding speed

Figure 9a exhibits how friction coefficient changes when the speed of the reciprocal pin is increased from 2.5 to 50 mm/s. The general behavior is that the friction coefficient increases with sliding speed. Furthermore, the tests done at 2.5 and 5 mm/s have the shorter running-in of about 1,250 cycles, and the lowest final friction values of 0.150 and 0.164, respectively. For the higher speeds, the running-in seems to take all the cycles, having final values for μ of 0.248 and 0.256, respectively.

In the case of sliding polymer/metal contacts, the speed also has an influence on the friction and wear of polymers and other polymeric composite materials (35). Our results demonstrate that the friction coefficient of Arboblend V2 Nature against a steel counterface increases with the sliding speed increase. The findings agree with reports of several industrial polymers sliding against metals ((45,48,49) and references therein). Lancaster has modeled the rise of surface temperature ΔT in the situation of polymers sliding against steel (50) as:

$$\Delta T = 5.7 \times 10^{-5} \mu H^{3/4} L^{1/4} V^{1/2} \quad (4)$$

where μ is the friction coefficient, L is the applied load (in N), H is the hardness (in Pa), and V is the siding speed (in m/s). A major source of error in ΔT calculations outlined by Lancaster in equation (4) is the assumption that the hardness is independent of temperature. If the temperature variation of H is included, Lancaster showed that equation (4) can be written as:

$$\Delta T = \Delta T_0 \exp(-0.00375\ \Delta T) \quad (5)$$

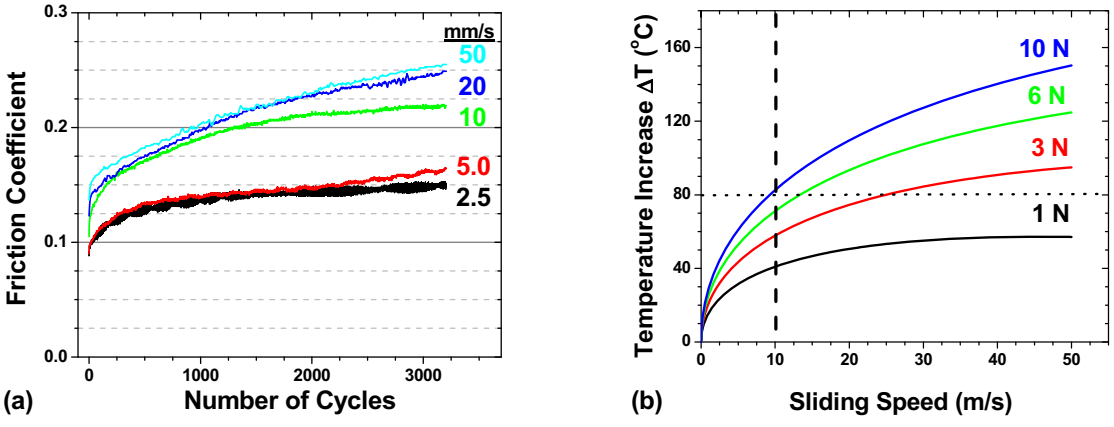

Figure 9: (a) Friction coefficient versus the number of cycles at $L = 3$ N measured at different sliding speeds; (b) increase of temperature at the contact area polymer/steel as a function of sliding speed for different applied loads.

where ΔT_0 is the temperature increase calculated assuming no change in hardness with temperature (i.e., equation (4)). Figure 9b displays the numerical solution of equation (5) for different loads. The model depicts the clear influence of load and speed. Taking into consideration that Arboblend V2 Nature softens at 103.7°C (14) and that the tribological experiments were done at 23°C, the horizontal dotted line at ΔT = 80°C indicates the limit where the material will start to melt. For the case of L = 3 N, we observe that for speeds below 10 m/s, the temperature never rises over the softening point, while for higher speeds, the temperature can rise up to 115°C. This data correlate well with the observed friction coefficient as a function of speed (Figure 9a). We can also observe the effect of load at V = 10 m/s (dashed vertical line in Figure 9b) which also correlates well with friction versus load (Figure 4) and especially wear versus load (Figure 6), where the material increases suddenly its wear at L = 6 N and L = 10 N: frictional heat could also be another factor influencing the increase of wear rate.

3.3.3 Influence of ambient humidity

Figure 10 uncovers the changes of friction coefficient as a function of ambient humidity. Both samples made at T = 160°C and 170°C have similar behavior for 0% and 35% HR. However, the friction coefficient measured at 75% show big differences: for samples made at T = 160°C, friction seems to start to increase at the end of the experiment while, for the sample made at 170°C, the friction curve has many irregularities and continue growing toward the end of the experiment.

Optical microscopy (Figure 11) reveals that the wear track for the experiment done at 0% RH has some plastic deformation but no visible wear, which is confirmed by the profile of the track in Figure 12. This unique feature can be linked to the high friction coefficient observed in our tests. When the humidity is increased to 75%, the track shows abrasion (Figures 11c and 12). The presence of abrasion correlates again with an increased friction coefficient.

After the seminal work of Reichenbach and Pourny in 1964 (51) and other subsequent publications, it is nowadays accepted that the atmospheric humidity has affected the friction and wear of certain polymers. In general, semicrystalline polymers like polyethylene terephthalate, polyamides (nylons), linear polyethylene, polytetrafluoroethylene, acetal (polyoxymethylene, POM), and isotactic polypropylene normally show only small variations in coefficients of friction in air, dry inert gases, or vacuum. In contrast, amorphous thermoplastics, such as PMMA, and polystyrene, and cross-linked thermosets, such as phenolics and epoxies, are more prone to environmental changes and appear to display higher friction in vacuum or dry inert gases than in air at medium RH. Hydrogen bonding to polymers containing free –OH groups could also be partially responsible in the observed increase of the friction coefficient in humid environments ((36,52–54) and references therein).

Only two investigations about the effect of humidity on Arboblend V2 Nature biopolymers have shown that the material adsorbs up to 6% of water (55) and that Arboblend V2 Nature does not contain –OH functions and only very small or no aromatic functions (14). Our results indicate that Arboblend V2 Nature behaves like other fossil-based thermoplastics, with more friction at 0% RH than at 33% RH. The high abrasion wear and friction coefficient observed at 75% RH could be a signal that the material lost part of its strength. More

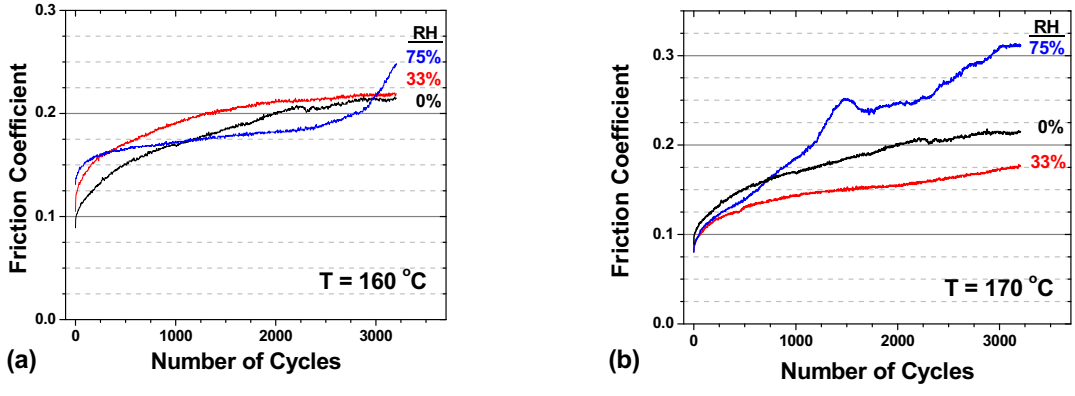

Figure 10: Friction coefficient versus the number of cycles at different relative humidity for samples made at (a) 160°C and (b) 170°C. The wear track is perpendicular to the textured lines of the surface.

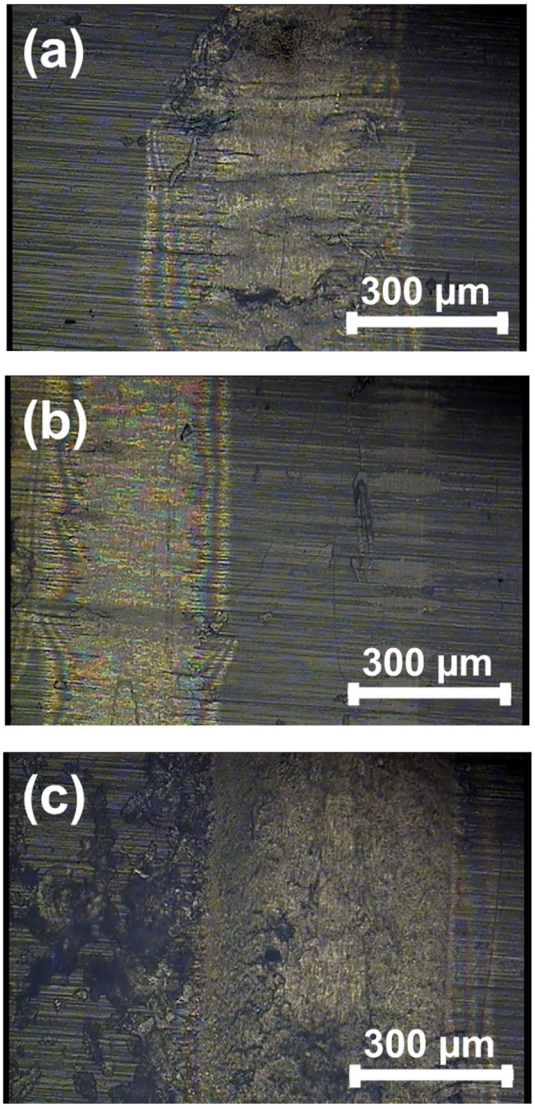

Figure 11: Optical microscopy of wear tracks produced at L = 3 N and (a) 0% RH; (b) 33% RH; and (c) 75% RH on samples made at T = 170°C. Wear tracks are perpendicular to the textured lines of the surface.

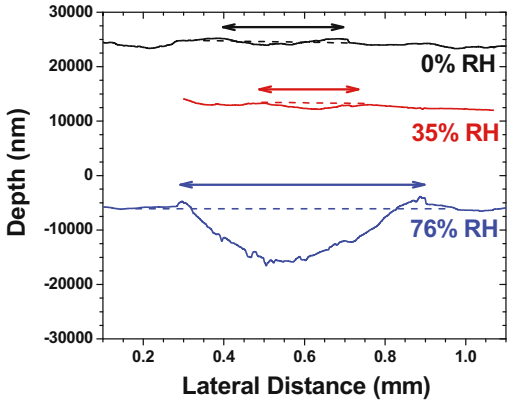

Figure 12: Wear track profiles obtained at different relative humidity (RH) for a specimen made at T = 170°C. Wear tracks are perpendicular to the textured lines of the surface.

investigation is needed to understand the stability of Arboblend V2 Nature material at very high humid environments.

4 Conclusions

The nanomechanics and tribology of Arboblend V2 Nature (a biopolymer consisting of >90% lignin, plus natural fibers, and additives) were measured according to the applied load, the sliding speed, and the ambient humidity. The specimens were made in real commercial production conditions by using an industrial-scale injection molding machine. Surface roughness is influenced by the melting temperature and the molding injection design. Nanoindentation tests have shown that the increase in temperature produces an increase in the Young's modulus and hardness. Tribological characterization has revealed that the friction coefficient increases with applied load or sliding speed. At applied loads of 1 N (contact pressure of 104 MPa) and tracks in a direction perpendicular to the textured lines, the lowest $\mu \sim 0.148$ are for samples made T = 170°C, while for tracks parallel to the textured lines, the lowest $\mu \sim 0.059$ is obtained for samples made at T = 160°C. Furthermore, in this paper, we studied for first time the influence of speed and ambient humidity on the tribology of lignin-based polymers A simple modeling indicates that frictional heat could be a factor influencing the increase of wear rate at high loads or high speeds. Like fossil-based thermoplastics, friction is found to be affected by ambient humidity, being the higher values at dry atmosphere or at very high (77%) RH; furthermore, samples measured at 6 and 10 N load present noticeable wear, which could be a signal that the material lost part of its strength.

Our results indicate that Arboblend V2 Nature biopolymers can be a successful candidate to replace some popular fossil-based thermoplastics in many tribological and mechanical applications.

Acknowledgments: E. Broitman acknowledges Prof. S. Grillo and Mr Hervè Glenat at the Laboratoire Procédés, Matériaux et Energie Solaire (PROMES-CNRS, France) for the use of the profilometer and tribometer in some of the experiments and for profitable discussions.

Conflict of interest: One of the authors (Esteban Broitman) is the Guest Editor of Special Issues and several articles published in e-Polymers.

References

(1) Biron M. Industrial Applications of Renewable Plastics: Environmental, Technological, and Economic Advances. Oxford: Elsevier; 2016.
(2) Sarkanen, S. The first alkylated 95–100% kraft lignin-based plastics. In: Ninth International Symposium on Wood and Pulping Chemistry. Montreal: CPPA; 1997.
(3) Sen S, Patil S, Argyropoulos DS. Thermal properties of lignin in copolymers, blends, and composites: a review. Green Chem. 2015;17(11):4862–87.
(4) Grossman A, Vermerris W. Lignin-based polymers and nanomaterials. Curr Opin Biotechnol. 2019;56:112–20.
(5) Höfer R. Sustainable Solutions for Modern Economies. Cambridge: RSC; 2009.
(6) Bioplastics News. Arboblend. [Online]. Available: https://bioplasticsnews.com/arboblend/. [Accessed 13 04 2020].
(7) Baden-Württemberg B. Thermoplastics made of lignin. Bioeconomy BW. 29 03 2010. (Online). Available: https://www.biooekonomie-bw.de/en/articles/pm/tecnaro-gmbh-thermoplastics-made-of-lignin. (Accessed 13 04 2020).
(8) Griffiths A. ArboSkin pavilion made from bioplastic by ITKE. De Zeen. 09 11 2013. [Online]. Available: https://www.dezeen.com/2013/11/09/arboskin-spiky-pavilion-with-facademade-from-bioplastics-by-itke/. [Accessed 13 04 2020].
(9) Kaeb H. Binabo and other sustainable toys. Bioplast Mag. 2019;14(3):13.
(10) TicToys. Binabo – more than a ball. TicToys GmbH, [Online]. Available: https://www.tictoys.de/en/products/binabo/. [Accessed 13 04 2020].
(11) Karlsson I. Materials for Application in the IKEA Decoration Range. Göteborg: Chalmers University of Technology; 2012.
(12) Lux N, Celotti M. Tecnaro. In: Green Brands Germany, Vol. IV. Veitsbronn: GB Organisation GmbH; 2019. p. 112–3.
(13) Bioplastics Australia. Arboblend. Allrounder [Online]. Available: https://biolastics.com.au/our-raw-materials/arboblend/. [Accessed 13 04 2020].
(14) Puiu E, Leontie L, Dumitraș M, Asandulesa M, Văideanu D, Petrescu TC. The thermodynamic behavior of liquid wood. Buletinul Institutului Politehnic Din Iaşi. 2018;64(1):201.
(15) Nedelcu D, Comăneci RI. Microstructure, mechanical properties and technology of samples obtained by injection from arboblend V2 nature. Indian J Eng Mater S. 2014;21(3):272–6.
(16) Nedelcu D, Stefan A, Mindru TD, Plavanescu S. Flexural properties of samples obtained from "liquid wood." Sel Eng Probl. 2012;3:151–4.
(17) Nedelcu D, Ciofu C, Lohan N. Microindentation and differential scanning calorimetry of liquid wood. Composites Part B. 2013;55:11–5.
(18) Broitman E, Nedelcu D, Mazurchevici S, Glenat H, Grillo S. Tribological and nanomechanical behavior of liquid wood. J Tribol-T ASME. 2019;141(2):022001.
(19) Oliver W, Pharr G. Measurement of hardness and elastic modulus by instrumented indentation: advances in understanding and refinements to methodology. J Mater Res. 2004;19(1):3–20.
(20) Díez-Pascual A, Gómez-Fatou M, Ania F, Flores A. Nanoindentation in polymer nanocomposites. Prog Mater Sci. 2015;67:1–94.
(21) Constantin C, Plăvănescu S, Nedelcu D. Impact comparative study of phone carcasses behavior by FEM. IOP Conf Ser Mater Sci. 2015;87:012100.
(22) Greenspan L. Humidity fixed points of binary saturated aqueous solutions. J Res Nat Bur Stand. 1977;81A(1):89–96.
(23) Pouzada A, Ferreira E, Pontes A. Friction properties of moulding thermoplastics. Polym Test. 2006;25:1017–23.
(24) Johnson B. The influence of processing on properties of injection-moulded and lomolded components. Stellenbosch: University of Stellenbosch; 2006.
(25) Sawyer LC. Polymer microscopy. Amsterdam: Springer Netherlands; 2017.
(26) The American Society of Mechanical Engineers. ASME B46.1-2009: Surface Texture (Surface Roughness, Waviness, and Lay). New York: The American Society of Mechanical Engineers; 2009.
(27) Broitman E. Indentation hardness measurements at macro-, micro-, and nanoscale: a critical overview. Tribol Lett. 2017;65:23.
(28) Flores A, Ania F, Baltá-Calleja FJ. From the glassy state to ordered polymer structures: a microhardness study. Polymer. 2009;50(3):729–46.
(29) La Carubba V, Brucato V, Piccarolo S. Influence of controlled processing conditions on the solidification of iPP, PET, and PA6. Macromol Symp. 2002;180:43–59.
(30) Maries GRD, Chira D, Bungau C, Costea T, Moldovan L. Determining the influence of the processing temperature by injection and of the subsequent pressure on the surface's hardness and indentation modulus of the products made of HDPE, PMMA, PC + ABS through nanoindentation. Mater Plast. 2017;54(2):214–20.
(31) Klein R. Material properties of plastics. In: Laser Welding of Plastics: Materials, Processes and Industrial Applications. Berlin: Wiley-VCH Verlag GmbH & Co.; 2011. p. 3–69
(32) Liparoti S, Speranza V, Sorrentino A, Titomanlio G. Mechanical properties distribution within polymer injection molded samples: effect of mold temperature under uneven thermal conditions. Polymers. 2017;9(11):585.
(33) Manenti S. Un'identità per I biopolimeri: il caso del legno liquido [Master Thesis]. Milan: Design Faculty of Politecnico di Milano; 2010.
(34) Broitman E. The nature of the frictional force at the macro-, micro-, and nano-scales. Friction. 2014;2:40–6.
(35) Abdelbary A. Wear of Polymers and Composites. Cambridge: Woodhead Publishing; 2015.
(36) Myshkin NK, Kovalev AV. Adhesion and friction of polymers. In: Sinha SK, Briscoe BJ, editors. Polymer Tribology. London: Imperial College Press; 2009. p. 3–37.
(37) McKeen LW. Fatigue and Tribological Properties of Plastics and Elastomers. Amsterdam: Elsevier; 2016; chapter 2.
(38) Hertz HR. Ueber die Beruehrung elastischer Koerper (On contact between elastic bodies). In: Gesammelte Werke (Collected Works), Vol. 1. Leipzig, Germany; 1895: 1882.

(39) Kar MK, Bahadur S. Micro-mechanism of wear at polymer-metal sliding interface. Wear. 1982;46(1):189–202.
(40) Yu C, Wang Q. Friction anisotropy with respect to topographic orientation. Sci Rep. 2012;2:988.
(41) Blau PJ. Friction Science and Technology: From Concepts to Applications. Boca Raton: CRC Press; 2008.
(42) Baum MJ, Heepe L, Gorb SN. Friction behavior of a microstructured polymer surface inspired by snake skin. Beilstein J Nanotechnol. 2014;5:83–97.
(43) Tramsen HT, Gorb S, Zhang H, Manoonpong P, Dai Z, Heepe L. Inversion of friction anisotropy in a bio-inspired asymmetrically structured surface. J R Soc Interface. 2018;15:20170629.
(44) Archard JF. Contact and rubbing of flat surfaces. J Appl Phys. 1953;24:981–8.
(45) Unal H, Sen U, Mimroglu A. Dry sliding wear characteristics of some industrial polymers against steel counterface. Tribol Int. 2004;37:727–32.
(46) Franklin SE. Wear experiments with selected engineering polymers and polymer. Wear. 2001;251:1591–8.
(47) Gu D, Zhang L, Chen S, Song K, Liu S. Significant reduction of the friction and wear of PMMA based composite by filling with PTFE. Polymers. 2018;10:966.
(48) Mimaroglu A, Unal H, Arda T. Friction and wear performance of pure and glass fiber reinforced poly-ether-imide on polymer and steel counterface materials. Wear. 2007;262:1407–13.
(49) Nuruzzaman D, Rahaman M, Chowdhury M. Friction coefficient and wear rate of polymer and composite materials at different sliding speeds. Int J Surf Sci Eng. 2012;6(3):231–45.
(50) Lancaster JK. Estimation of the limiting PV relationships for thermoplastic bearing materials. Tribology. 1971;4(2):82–86.
(51) Reichenbach GS, Poumy JL. The importance of humidity in friction measurement. Lubr Eng. 1964;20:409–13.
(52) Hetemi D, Pinson J. Surface functionalisation of polymers. Chem Soc Rev. 2017;46:5701–13.
(53) Jenkins AD. Polymer Science: A Materials Science Handbook. Amsterdam: North Holland; 2013.
(54) Lancaster JK. A review of the influence of environmental humidity and water on friction, lubrication and wear. Tribol Int. 1990;23(6):371–89.
(55) Barhalescu ML, Ghita S, Petrescu TC. The risk of liquid wood degradation under the influence of marine factors. MATEC Web Conf. 2019;290:12012.